Journal of Engineering Science and Technology
Vol. 13, No. 4 (2018) 909 - 924

MAXIMIZATION OF COOLING EFFECTIVENESS OF TURBINE BLADE SURFACES USING DIFFERENT ARRANGEMENT OF COOLING HOLES AND VARIOUS BLOWING RATIOS

MADHURIMA DEY[1], PRAKHAR JINDAL[1], APURBA KUMAR ROY[2], KAUSHIK KUMAR[2,*]

[1]Research Scholar, Birla Institute of Technology, Mesra, Ranchi, Jharkhand, 835215, India
[2]Associate Professor, Birla Institute of Technology, Mesra, Ranchi, Jharkhand, 835215, India
*Corresponding Author Email: kkumar@bitmesra.ac.in

Abstract

In gas turbines, the operating temperature of the primary fluid is very high. In order to lessen the damage of turbine blades due to severe working temperature, film cooling holes are commonly implemented during designing of turbine blades. Film cooling effectiveness has been studied numerically to determine the arrangement of cooling holes and optimum blowing ratio. In this study, three dimensional standard Reynold's Average Navier Stokes (RANS) shear stress transport turbulence model have been used for the simulation purpose. Three different shapes of cooling holes have been considered to find out optimum shape of the hole geometry. The blowing ratios equal to 0.2, 0.4, 0.6, 0.8 and 1.0 and the free stream Reynolds number based on the free stream velocity and hydraulic diameter of the mainstream channel as 15316have been taken for the present study. 3D domain has been used in order to capture recirculation zone near the wall. Effectiveness obtained for fan-shaped hole at M = 0.8 and 1 is maximum compared to conventional hole shapes. Film cooling effectiveness is highest near the hole region which decreases further downstream of cooling holes due to coolant and mainstream intermixing. The simulation results show that best effective blade surface cooling is achieved for fan-shaped staggered row at blowing ratio equal to 1.0.

Keywords: Film cooling effectiveness, Fan-shaped hole, Blowing ratio.

1. Introduction

The functioning temperature of the main fluid in gas turbines is very high. The blades of turbine may break down because of severe operational temperature.

Nomenclatures

D	Diameter (m)
K	Turbulent kinetic energy
M	Blowing ratio
$\underline{\mathrm{Re}}_D$	Reynolds number based on hydraulic diameter
T_{aw}	Adiabatic wall temperature (K)
$T_{c,exit}$	Coolant temperature (K)
T_∞	Mainstream temperature (K)
U_c	Coolant velocity (m/s)
U_∞	Mainstream velocity (m/s)
x/D	Position at x-axis to diameter ratio
y/D	Position at y-axis to diameter ratio

Greek Symbols

E	Turbulence dissipation
H	Film cooling effectiveness
Ω	Specific dissipation rate

Abbreviations

NH_3	Ammonia
RANS	Reynolds Averaged Navier Stokes

Hence, to minimize the detrimental effect on turbine blades, cooling holes are generally integrated during turbine blade designs. Film cooling involves bleeding of cool air from the compressor then it is ducted to more than one internal chamber of the turbine blades. Coolant from internal chamber is discharged through cooling holes thus forming cooling jets resulting in reduced convective heat transfer to the surface of the turbine blades.

Studies on enhancing heat transfer coefficients incorporating Rayleigh number effects and better lateral spreading of injected coolant carried out by lacovides and Launder [1] and Gritsch et al. [2]. Nikpatro and Schobeiri [3] performed experiments on a highly loaded low-pressure turbine blade under steady and unsteady wake flow conditions to determine the effect of flow separation and pressure gradient on film-cooling effectiveness. Moreover, the effect of impinging wakes on the overall film coverage of blade surfaces was studied by them. They have found that heat transfer coefficient and film-cooling effectiveness in majority of regions behaved in opposite ways.

Bohn et al. [4] studied influence of heat transfer within the cooling film and found that local heat transfer rate varies significantly depending on the local position. Kadja and Bergelest [5], Yuen and Botas [6], Hasan and Puthukkudi [7] and Dey et al. [8] found that effective blade surface cooling can be achieved when the blowing ratio was increased but cycle efficiency was reduced. Feng et al. [9] used the k-ε turbulence model and found secondary flow near the blade surface in the wake region behind the jet hole. Tao et al. [10] found that standard k-ε model gave poorest results whereas k-ω and SST k-ω turbulence model gave better results and produced closer estimation for pressure side and suction side due to isotropic characteristics.

Liu et al. [11] used realizable k-ε model with one-Eq. model in near wall region and observed that reducing turbulent Prandtl number increased film cooling effectiveness under large blowing ratio.

Baheri et al. [12], Lee and Kim [13] and Schroeder and Thole [14] studied the film cooling effectiveness with various shaped holes. It was found that an increase in forward expansion angle reduces film-cooing effectiveness and the penetration of jet into the mainstream is high at higher blowing ratio resulting in presence of counter rotating vortex pair in the flow-field, thus increased lateral spreading of coolant which was found by Rozati and Tafti [15] as well.

Yong et al. [16] used NH_3 as coolant with different blowing ratios and found an improvement in film cooling effectiveness in stream-wise and span-wise direction. Montomoli et al. [17] studied numerically as well as experimentally a new film cooling geometry with high pitch to diameter ratio and found that effectiveness increased by 30%.

Johnson et al. [18] used Particle Image Velocimetry (PIV) system and Pressure Sensitive Paint (PSP) technologies to conduct an experimental study. They found that film cooling effectiveness increased with increase in density ratios and coolant jet flows separated from test plate at low density ratio in spite of injection of large amount of coolant which lowered film cooling effectiveness. Nikpatro and Schobeiri [19] have provided an elaborative discussion on various turbulence models used for film cooling effectiveness in their work.

From the existing literatures, it can be concluded that designing of film cooling holes is a big challenge for effective cooling of turbine blade surfaces as gas turbine airfoil film cooling gets greatly affected by a number of variables. The prominent amongst those is the arrangement and configuration of discrete coolant holes for cooling turbine airfoils and end walls, and this was the background and primary focus of this work. Hence this study aims at determining the arrangement of cooling holes and blowing ratio which produce the maximum film cooling effectiveness. Numerical analysis has been carried out to find the effective way of cooling turbine blades. The standard RANS shear stress transport turbulence model has been used for the computational analysis using ANSYS software.

2. Methodology

2.1. Computational model

Figure 1 represents two dimensional side view of the flow domain of the present analysis. The height in z-direction of the main-flow inlet is 10*D* similar to the work of Hasan and Puthukkudi [7]. The width in y-direction of flat plate is equal to 20*D*. '*D*' is the diameter of circular hole equal to 5 mm. For the ease of manufacturability, fan-shaped hole has circular cross-section at the inlet and fan-shaped at the outlet. Fan-shaped holes are known to have expanded exits as the exit area is equal to three times the entry area which has been given by Gritsch et al. [2]. The present study is regarding analysis of film cooling effectiveness from fan-shaped single row and fan-shaped staggered row at different blowing ratios. Figure 2 shows the geometrical configuration of single and staggered row.

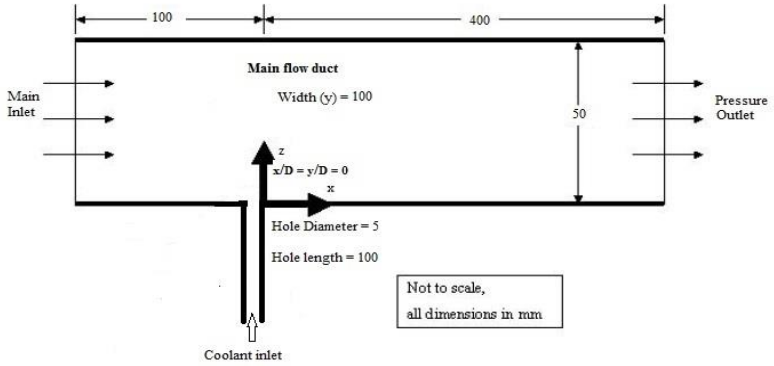

Fig. 1. Domain and coordinates.

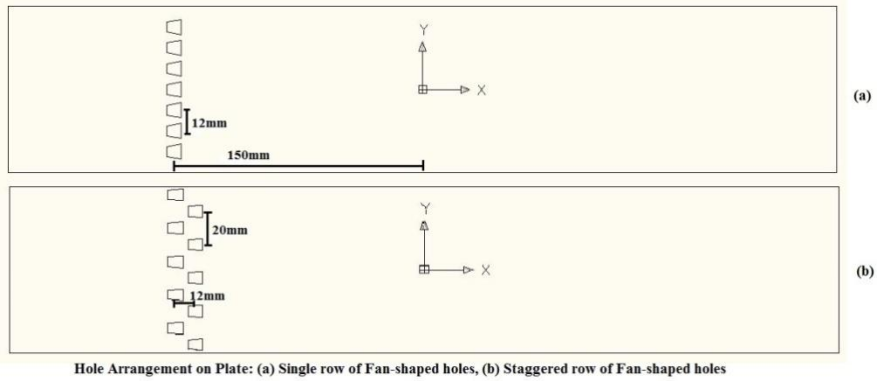

Fig. 2. Configurations of hole arrangement.

2.2. Mathematical equations

The film cooling performance is characterized by a non-dimensional parameter known as Film cooling effectiveness. It is defined as the ratio of temperature difference between mainstream and adiabatic wall to the temperature difference between mainstream and coolant which can be found in Kadja and Bergelest [5], Yuen and Botas [6] and many other literatures. Film cooling effectiveness is given by Eq. (1).

$$\eta = \frac{(T_\infty - T_{aw})}{(T_\infty - T_C)} \tag{1}$$

As it has been mentioned earlier, in the present study, The Reynolds Stress Model (RSM) has been used. The Reynolds Stress Model (RSM), also called as the Reynolds Stress Transport Model, is a higher level turbulence model. Here the closure employed is commonly called a second order closure. In Reynolds stress model (RSM), the calculation of the individual Reynolds stresses, $\rho\overline{u_i' u_j'}$ are being done using differential transport Equations. The individual Reynolds stresses are

used to obtain the closure of the Reynolds-averaged momentum Equation. The salient and pertinent Eqs. (2-11), used in the present work for Reynolds Stress Model mathematical formulation (ANSYS. Inc., 2009) [20], are given below.

The transport Eq. (2) for Reynolds stresses, $\overline{u_i^{'}u_j^{'}}$ **,** can be written as:

$$\frac{\partial}{\partial t}\left(\rho\overline{u_i^{'}u_j^{'}}\right)+\frac{\partial}{\partial x_k}\left(\rho u_k\overline{u_i^{'}u_j^{'}}\right)=-\frac{\partial}{\partial x_k}\left[\rho\overline{u_i^{'}u_j^{'}u_k^{'}}+\overline{\rho^{'}\left(\delta_{kj}u_i^{'}+\delta_{ik}u_j^{'}\right)}\right]$$
$$+\frac{\partial}{\partial x_k}\left[\mu\frac{\partial}{\partial x_k}\left(\overline{u_i^{'}u_j^{'}}\right)\right]-\rho\left(\overline{u_i^{'}u_k^{'}}\frac{\partial u_j}{\partial x_k}+\overline{u_j^{'}u_k^{'}}\frac{\partial u_i}{\partial x_k}\right) \quad (2)$$
$$+\overline{\rho^{'}\left(\frac{\partial u_i^{'}}{\partial x_j}+\frac{\partial u_j^{'}}{\partial x_k}\right)}-2\mu\overline{\frac{\partial u_i^{'}}{\partial x_k}\frac{\partial u_i^{'}}{\partial x_k}}$$
$$+2\rho\Omega_k\left(\overline{u_j^{'}u_m^{'}}\varepsilon_{ikm}+\overline{u_i^{'}u_m^{'}}\varepsilon_{jkm}\right)$$

The above Eq. (1) can be written as, Local time derivative + C_{ij} = $D_{T,ij}$ + $D_{\mathrm{L},ij}$ + P_{ij} + ϕ_{ij} - ε_{ij} + F_{ij} where C_{ij} is the Convection-Term, $D_{T,ij}$ stands for Turbulent Diffusion,, $D_{\mathrm{L},ij}$ is the Molecular Diffusion,, P_{ij} stands for Stress Production,, ϕ_{ij} is for the Pressure Strain,, ε_{ij} is the Dissipation and F_{ij} is for Production by System Rotation. Among these terms, C_{ij} , $D_{\mathrm{L},ij}$, P_{ij} **,** and F_{ij} do not require modelling. However, $D_{T,ij}$, ϕ_{ij} , and ε_{ij} are required to be modelled for closing the equations. The correctness of the Reynolds stress model depends on the accuracy of the models for the turbulent transport, the pressure-strain correlation and the dissipation terms.

The Turbulent Diffusion term is required to be modelled by the following Eq. (3).

$$D_{T,ij}=\frac{\partial}{\partial x_k}\left(\frac{\mu_\tau}{\sigma_k}\frac{\partial\overline{u_i^{'}u_j^{'}}}{\partial x_k}\right) \quad (3)$$

The Turbulent viscosity term μ_τ can be computed using Eq. (4).

$$\mu_\tau=\rho C_\mu\frac{k^2}{\varepsilon} \quad (4)$$

where the value of C_μ = 0.09 and σ_k = 0.82.

The Pressure Strain term ϕ_{ij} of Eq. (1) can be written as shown in Eq. (5).

$$\phi_{ij}=\phi_{ij,1}+\phi_{ij,2}+\phi_{ij,w} \quad (5)$$

where $\phi_{ij,1}$ is the slow pressure-strain term, $\phi_{ij,2}$ is called the rapid pressure-strain term and $\phi_{ij,w}$ is the wall reflection term. The term $\phi_{ij,w}$ is responsible for the redistribution of normal stresses vicinity of the wall. The wall reflection term

tends to damp the normal stress normal to the wall, enhancing the stresses parallel to the wall. This term is modelled using Eq. (6).

$$\phi_{ij,w} \equiv C_1^{'} \frac{\varepsilon}{k}\left(\overline{u_k^{'}u_m^{'}}n_k n_m \delta_{ij} - \frac{3}{2}\overline{u_i^{'}u_k^{'}}n_j n_k - \frac{3}{2}\overline{u_j^{'}u_k^{'}}n_i n_k\right)\frac{C_l k^{\frac{3}{2}}}{\varepsilon d}$$
$$+C_2^{'} \frac{\varepsilon}{k}\left(\phi_{km,2}n_k n_m \delta_{ij} - \frac{3}{2}\phi_{ik,2}n_j n_k - \frac{3}{2}\phi_{jk,2}n_i n_k\right)\frac{C_l k^{\frac{3}{2}}}{\varepsilon d} \quad (6)$$

where $C_1^{'}$ = 0.5, $C_2^{'}$ = 0.3. Here n_k is the x_k component of the unit normal to the wall, d stands for the normal distance to the wall, and $C_l = C_\mu^{3/4} / \mathrm{k}$, where C_μ = 0.09 and k is the von Karman constant (= 0.4187).

While modelling the turbulence kinetic energy for a specific term, it is obtained by taking the trace of the Reynolds stress tensor which is shown in Eq. (7).

$$k = \frac{1}{2}\overline{u_i^{'}u_j^{'}} \quad (7)$$

The dissipation tensor, ε_{ij} , is modelled using the Eq. (8).

$$\varepsilon_{ij} = \frac{2}{3}\delta_{ij}\left(\rho\varepsilon\right) \quad (8)$$

The scalar dissipation rate, ε is computed with a model transport Eq. using Eq. (9).

$$\frac{\partial}{\partial t}\left(\rho\varepsilon\right) + \frac{\partial}{\partial x_i}\left(\rho\varepsilon u_i\right) = \frac{\partial}{\partial x_j}\left[\left(\mu + \frac{\mu_t}{\sigma_\varepsilon}\right)\frac{\partial\varepsilon}{\partial x_j}\right] C_{\varepsilon 1}\frac{1}{2}\left[P_{ii} + C_{\varepsilon 3}G_{ii}\right]\frac{\varepsilon}{k}$$
$$-C_{\varepsilon 2}\rho\frac{\varepsilon^2}{k} + S_\varepsilon \quad (9)$$

where σ_ε = 1.0, $C_{\varepsilon 1}$ = 1.44, $C_{\varepsilon 2}$ = 1.92. Here $C_{\varepsilon 3}$ is evaluated as a function of the local flow direction relative to the gravitational vector. S_ε is a user defined source term and G_{ii} is referred as production term due to buoyancy.

Along with the Reynolds stress model**,** the turbulent heat transport is modelled using the concept of Reynolds' analogy to turbulent momentum transfer. The modelled energy Eq. is shown the Eq. (10).

$$\frac{\partial}{\partial t}\left(\rho E\right) + \frac{\partial}{\partial x_i}\left[u_i\left(\rho E + p\right)\right] = \frac{\partial}{\partial x_j}\left[\left(k + \frac{c_p\mu_t}{\mathrm{Pr}_t}\right)\frac{\partial T}{\partial x_j} + u_i\left(\tau_{ij}\right)_{eff}\right] + S_h \quad (10)$$

where E is the total energy and $\left(\tau_{ij}\right)_{eff}$ is the deviatoric stress tensor. The expression for $\left(\tau_{ij}\right)_{eff}$ of Eq. (10) shown in Eq. (11).

$$\left(\tau_{ij}\right)_{eff} = u_{eff}\left(\frac{\partial u_j}{\partial x_i} + \frac{\partial u_i}{\partial x_j}\right) - \frac{2}{3}\mu_{eff}\frac{\partial u_k}{\partial x_k}\delta_{ij} \tag{11}$$

In Eq. (10), the term $\left(\tau_{ij}\right)_{eff}$ represents heating due to the viscous action and is always computed in the density-based solvers. The most common value of Prandtl number, Pr_t, is 0.85.

2.3. Boundary conditions

The mainstream and coolant has been used as air. The mainstream hot air is at 600K with a velocity inlet boundary condition equal to 25m/s flowing through main inlet from left to right and has been kept fixed for all the cases. The boundary condition specified to main outlet is pressure outlet. The coolant air is at 300K and its velocity has been calculated corresponding to each blowing ratios which are 0.2, 0.4, 0.6, 0.8 and 1.0. The coolant hole is inclined at angle of 90^o with velocity inlet as boundary condition at coolant inlet. The lower wall and coolant outlet have been given interface as boundary condition. The wall boundary condition has been set for upper wall, side walls and coolant wall. Blowing ratio (*M*) is the ratio of coolant to mainstream mass flux and is given by Eq. (12) below.

$$M = \frac{\rho_c U_c}{\rho_\infty U_\infty} \tag{12}$$

2.4. Computational details

Modelling and simulation has been performed on Gambit and Fluent 14. Throughout the study, hexahedral cells have been used for better accuracy. The RANS shear stress transport model has been used for the simulation work as the model is directly utilizable at the wall through the viscous sub-layer and give better results for near wall conditions as found out by Tao et al. [10]. Pressure based type solver has been used with SIMPLE algorithm. Second order high resolution method has been adopted for the discretization of continuity, momentum, turbulent kinetic energy, and rate of dissipation of turbulent kinetic energy and energy equations. When the residual quantities are less than 10^{-3} for continuity, 10^{-3} for momentum and 10^{-6} for energy, then the convergence criterion have been achieved. Figure 3 shows the computational domain of the model. Figure 4 shows near wall mesh which is hybrid in nature.

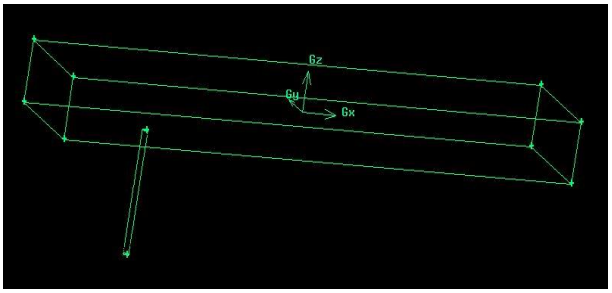

Fig. 3. Computational model.

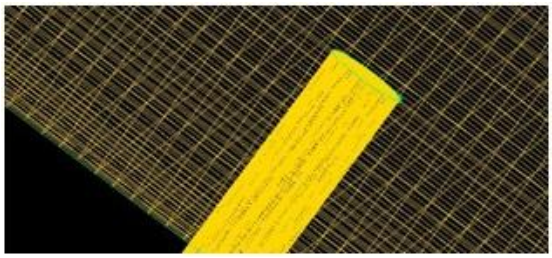

Fig. 4. Near wall mesh.

2.5. Validation and grid dependency test

The present work has been validated using single circular hole case at blowing ratio (*M*) equal to 0.6 and compared with the experimental literature of Yuen and Botas [6] and is shown in Fig. 5. The obtained computational result which is centerline effectiveness is almost similar to the experimental results achieved by Yuen and Botas [6] for cylindrical hole at an angle of 90^{o}. The grid independence test was carried out and shown in Fig. 6. The size of coarse grid is 25, 50, 000, medium grid is 28, 38, 225 and fine grid is 30, 50, 000 hexahedral cells respectively.

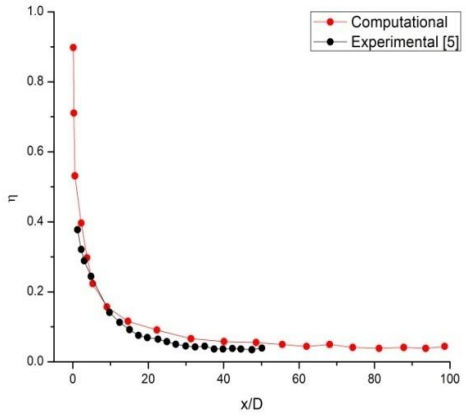

Fig. 5. Effectiveness for circular hole at blowing ratio M = 0.6.

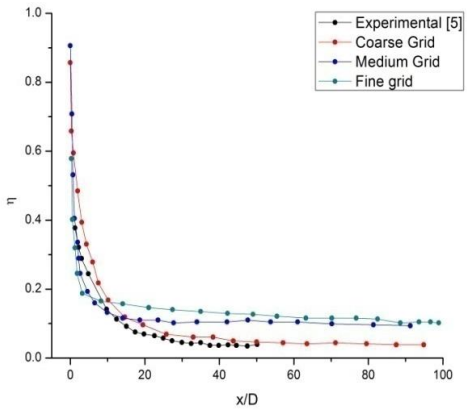

Fig. 6. Grid dependency test.

3. Results and Discussion

Averaged film cooling effectiveness at different blowing ratios (*M*) equal to 0.2, 0.4, 0.6, 0.8 and 1.0 for single hole (circular, square and fan-shaped hole) has been compared as shown in Fig. 7. It shows that maximum effectiveness is obtained at *M* = 0.4 and 0.2 for circular hole shape and square hole shape respectively. Fan-shaped hole gives maximum effectiveness at all blowing ratios compared to conventional hole shapes. Highest effectiveness for fan-shaped hole is obtained at *M* = 0.8 and 1.0. Thus, further comparisons are based on fan-shaped hole at *M* = 0.8 and 1.0 for different arrangement of holes.

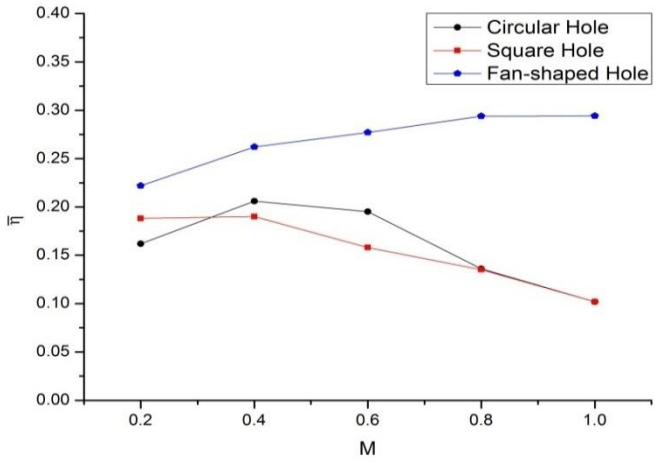

Fig. 7. Averaged film cooling effectiveness versus blowing ratios for different hole shapes.

Figures 8(a) and (b) show spatial effectiveness for fan-shaped single row at an axial distance of 400 mm from the leading edge of plate for *M* = 0.8 and 1.0 respectively. Results show that effectiveness is maximum near the hole region which decreases further downstream of cooling holes. These heights represent the coolant jet path and where there is no cooling holes effectiveness is equal to zero. Thus, at the mid-span of two cooling holes effectiveness is zero.

Figures 8(c) and (d) show spatial effectiveness for fan-shaped staggered row at an axial distance of 400 mm from the leading edge of plate for *M* = 0.8 and 1.0 respectively. Results show that effectiveness has increased for staggered row which is almost approaching 1.0. In case of staggered row, larger area of plate is cooled as well as uniform cooling of plate takes place compared to single row. Effectiveness is maximum near hole area whereas further downstream it decreases.

Figures 9 and 10 show comparison of spatial effectiveness for fan-shaped single and staggered row at *x/D* equal to -20 for *M* = 0.8 and 1.0. The film cooling effectiveness decreases after a certain length from the cooling holes due to increase in intermixing between coolant and mainstream. The value *x/D* = -20 has been taken because after that position film cooling effectiveness decreases significantly. As coolant quantity is also a constraint, hence *x/D* = -20 is the

maximum length which has been cooled effectively. Results show that effectiveness for single row is almost same for both the blowing ratios with maximum effectiveness approaching 0.6. In case of staggered row, maximum effectiveness is obtained for blowing ratio equal to 1 almost equal to 0.65. Plate is cooled uniformly over the entire area compared to single row. Effectiveness is zero at the edges for single row due to absence of cooling holes.

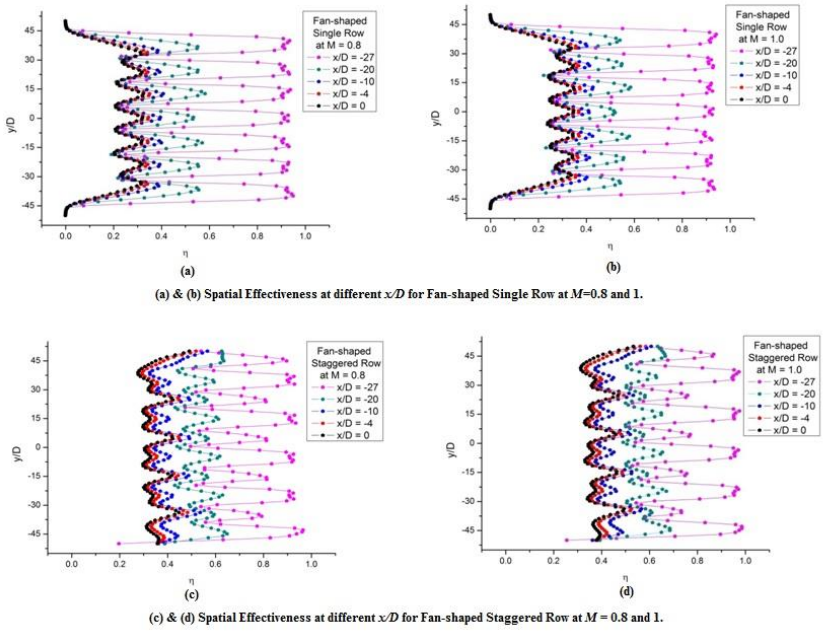

(a) & (b) Spatial Effectiveness at different x/D for Fan-shaped Single Row at M=0.8 and 1.

(c) & (d) Spatial Effectiveness at different x/D for Fan-shaped Staggered Row at M = 0.8 and 1.

Fig. 8. Spatial effectiveness at different x/D for fan-shaped single and staggered row at M = 0.8 and 1.0.

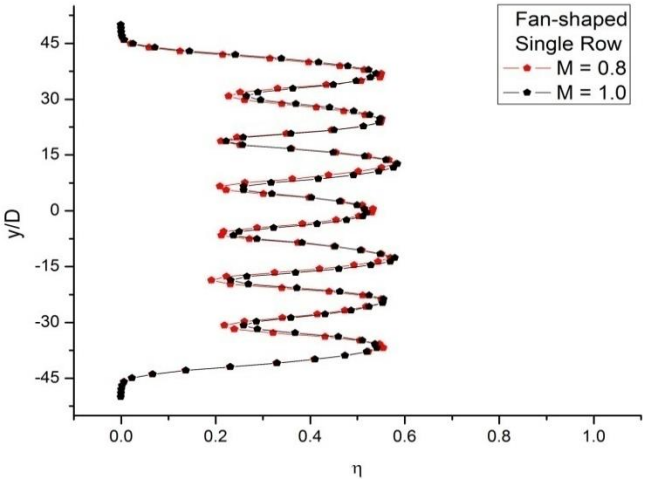

Fig. 9. Spatial effectiveness at x/D = -20 for fan-shaped single row at different blowing ratios.

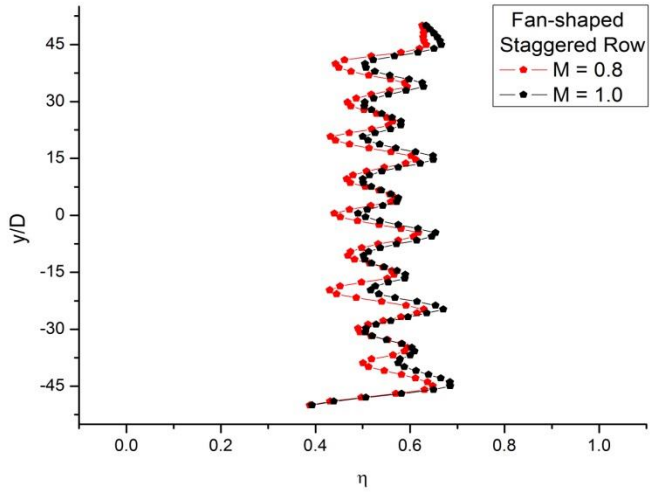

Fig. 10. Spatial effectiveness at *x/D* = -20 for fan-shaped staggered row at different blowing ratios.

Figures 11 and 12 show comparison of spatially averaged effectiveness for fan-shaped single and staggered row for M = 0.8 and 1.0. Results show that maximum effectiveness for single row almost approaches to unity at *x/D* equal to -20 whereas average effectiveness is 0.75 for both the blowing ratios. Maximum effectiveness is obtained for M = 1.0 further downstream of cooling holes. In case of staggered row, maximum effectiveness is equal to unity and average effectiveness almost approaches to 0.8 at *x/D* equal to -20 for blowing ratio 1.0. Entire plate is cooled effectively with average effectiveness greater than 0.35. Maximum effectiveness is obtained for M = 1.0 near the cooling hole as well as further downstream of cooling holes.

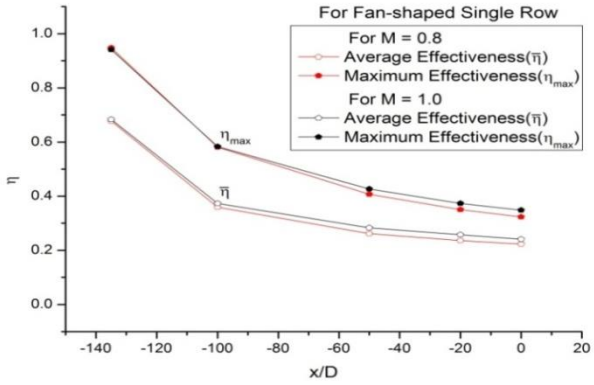

Fig. 11. Spatially averaged effectiveness at *x/D* = -20 for fan-shaped single row at different blowing ratios.

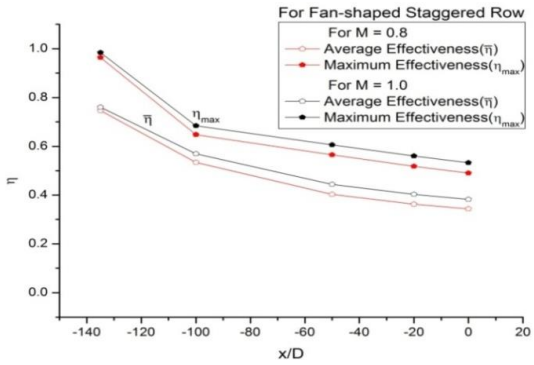

Fig. 12. Spatially averaged effectiveness at *x/D* = -20 for fan-shaped staggered row at different blowing ratios.

Figures 13(a) and (b) show temperature and velocity contours for different single hole shapes at M = 1.0. Temperature of the hot plate almost approaches 300K near the hole surface. There is formation of recirculation zone near the hole and it spreads laterally but does not affect the coolant flow path downstream of the cooling holes. As it is clear from the figure that coolant flow path is smooth.

Figures 14 and 15 represent temperature contours for fan-shaped single row and staggered row at M = 0.8 and 1.0. Entire plate is cooled in fan-shaped staggered row comprising of 10 holes compared to single row which comprises of 7 holes.

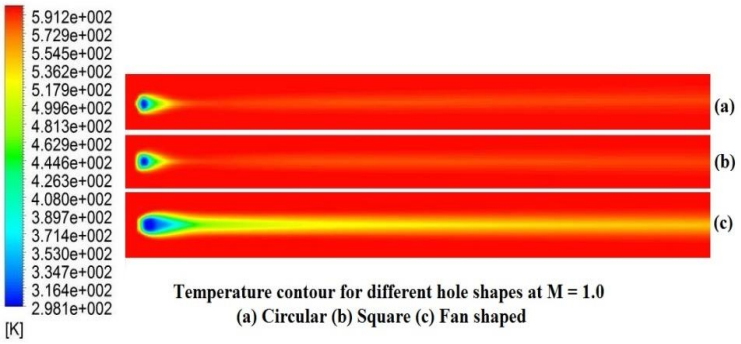

(A) Temperature contour.

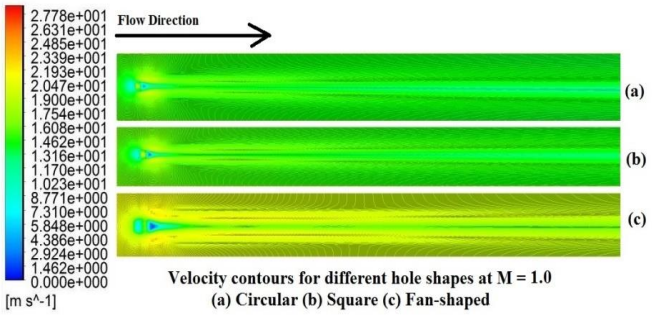

(B) Velocity contour.

Fig. 13. Temperature and velocity contour for single hole shapes at *M* = 1

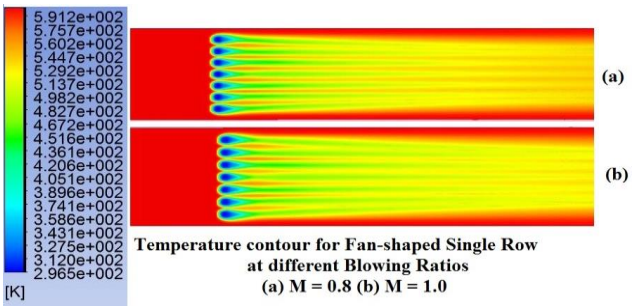

Fig. 14. Temperature contour for fan-shaped single row at different blowing ratios.

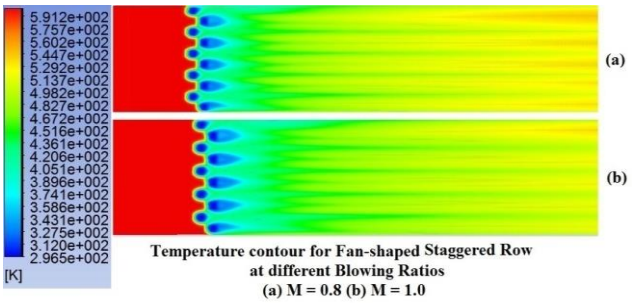

Fig. 15. Temperature contour for fan-shaped staggered row at different blowing ratios.

Figure16 shows recirculation zone formed near the wall for circular, square and fan-shaped hole at blowing ratio equal to 1.0. It is clear from the result that recirculation of coolant near the wall is minimum for fan-shaped hole and maximum for circular hole. The recirculation of coolant spreads laterally and deteriorates the film cooling effectiveness. In order to capture recirculation zone formed near the wall, three-dimensional domain has been used instead of two dimensional domain for the study. Thus, result reveals that recirculation of coolant is reduced in fan-shaped hole compared to conventional hole shapes that are circular and square holes.

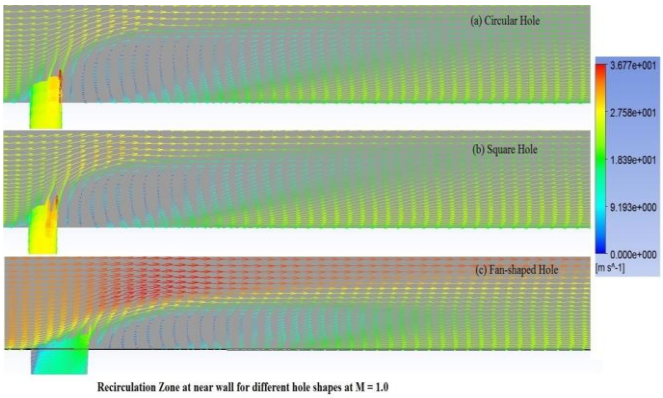

Fig. 16. Recirculation zone at near wall for single hole shapes at *M* = 1.0.

4. Conclusions

An effective cooling technique is essential for Gas turbine blades as they are exposed to high inlet temperature and usage of the same substantially provides protection from developed thermal stresses. The performance of film-cooling is determined by the fact whether the coolant jet gets separated from the surface or not. For nominal conditions of flat surfaces, low free stream turbulence, and cylindrical holes, the film-cooling performance can be closely predicted using empirical correlations but for noncircular hole geometry, formulation and efficacy of empirical correlations is difficult to achieve. Hence shaping of the hole exit along with blowing ratio can greatly alter film-cooling performance. Although CFD is considered to be very useful tool in predicting and providing the detailed insight mechanism of the film-cooling process it has also limitation due to very complex flow conditions that occur for film cooling, especially in the situation when the coolant jets starts separating. So under the circumstances effectiveness of film-cooling performance for actual turbine conditions is often quite tough for accurate prediction, and this remains a major constraint in the design for the durable performance of the turbine section. In this work numerical investigation on the film cooling effectiveness has been carried out to determine the arrangement of cooling holes and optimum blowing ratio using Reynold's Average Navier Stokes (RANS) shear stress transport turbulence model. The blowing ratios (M) equal to 0.2, 0.4, 0.6, 0.8 and 1.0 and the free stream Reynolds number (Re_D) based on the free stream velocity and hydraulic diameter of the mainstream channel as 15316 have been considered for the present study. Following conclusions can be made from the observations obtained from the study:

- The turbulence model chosen for the present numerical investigation shows a good agreement with the available experimental results in the published literature. It indicates the correctness of the chosen model i.e. Reynold's Average Navier Stokes (RANS) shear stress transport turbulence model for the analysis.
- Film cooling effectiveness for circular holes is found to be less as compared to the fan-shaped holes. In fan-shaped holes, the cooling effectiveness is larger because of expansion of the jet at exit of the hole. As the jet spreads, velocity decreases at exit and thus coolant gets enough time to stay near the hole surface on the plate ensuring better thermal barrier. This also reduces the probability of the occurrence of coolant jet to get separated or 'lift off" from the surface ensuring better and effective film cooling.
- Film cooling effectiveness not only depends on the hole geometry but also largely depends on arrangement of holes. By choosing appropriate arrangement of cooling holes, one can enhance the overall effectiveness of the same. It is observed from the present study that film cooling effectiveness along the lateral direction for single row coolant holes show steeper and discrete wavy pattern as compared to double row staggered holes for all blowing ratios. This may be attributed to the fact that double row staggered holes spreads the coolant in a uniform way along the lateral direction as compared to single row, hence allowing better protection of the blade surfaces from high temperature primary fluids. For all cases the film cooling effectiveness increases with the increase in blowing ratios and at blowing ratio near to unity, film cooling effectiveness was found to be maximum in

the present investigation. Using the present hole arrangement improvement in film cooling effectiveness has been observed and the same can be applied to industrial problems.

5. Future Work

In the present work in order to determine the arrangement of cooling holes and blowing ratio to produce the maximum film cooling effectiveness, the density of the air has been assumed to be constant along the length of the plate but in actual practice, due to a temperature gradient, density also changes from one end to the other end. Hence for a more practical and real time solution this change requires to be incorporated in the boundary conditions.

Acknowledgement

The authors sincerely acknowledge the comments and suggestions of the reviewers that have been instrumental for improving and upgrading the paper in its final form.

References

1. Iacovides, H.; and Launder, B.E. (1995). Computational fluid dynamics applied to internal gas-turbine blade cooling: A review. *International Journal Heat and Fluid Flow*, 16(6), 454-470.
2. Gritsch, M.; Schulz, A.; and Wittig, S. (2001). Film-cooling holes with expanded exits: near hole heat transfer coefficients. *International Journal Heat and Fluid Flow*, 21(2), 146-155.
3. Nikpatro, A. and Schobeiri, M.T. (2017). Experimental investigation of film-cooling effectiveness of a highly loaded turbine blade under steady and periodic unsteady flow conditions. *Journal of Heat Transfer*, 139(7), 1-13.
4. Bohn, D.; Ren, J. and Karsten Kusterer, K. (2005). Systematic investigation on conjugate heat transfer rates of film cooling configurations. *International Journal of Rotating Machinery*, 3, 211-220.
5. Kadja, M. and Bergelest, G. (1997). Computational study of turbine blade cooling by slot-injection of gas. *Applied Thermal Engineering*, 17(12), 1141-1149.
6. Yuen, C.H.N. and Martinez-Botas, R.F. (2003). Film cooling characteristics of a single round hole at various streamwise angles in a crossflow: Part I Effectiveness. *International Journal of Heat and Mass Transfer*, 46(2), 221-235.
7. Hasan, R. and Puthukkudi, A. (2013). Numerical study of effusion cooling on an adiabatic flat plate. *Propulsion and Power Research*, 2(4), 269-275.
8. Dey, M.; Jindal, P.; Roy, A.K. and Kumar, K. (2016) Effect of geometry and array of cooling holes in film cooling over an adiabatic flat plate - a computational approach. *REST Journal on Emerging trends in Modelling and Manufacturing*, 2(1), 10 - 20.

9. Feng, Y.; Xiao-Cheng, Z. and Zhao-hui, D. (2007). Experimental measurement and numerical simulation for flow field and film cooling effectiveness in film-cooled turbine. *Journal of Hydrodynamics*, Ser. B, 19(4), 459-466.
10. Tao, Z.; Zheo, Z.; Ding, S; Xu, G. and Wu, H. (2009). Suitability of three different two-Eq. turbulence models in predicting film cooling performance over a rotating blade. *International Journal of Heat and Mass Transfer,* 52(5-6), 1268-1275.
11. Liu, C.; Zhu, H. and Bai, J. (2008). Effect of turbulent Prandtl number on the computation of film-cooling effectiveness. *International Journal of Heat and Mass Transfer,* 51(25-26), 6208-6218.
12. Baheri, S.; Alavi Tabrizi, S.P. and Jubran, B.A. (2008). Film cooling effectiveness from trenched shaped and compound holes. *Heat Mass Transfer*, 44(8); 989-998.
13. Lee, K. and Kim, K. (2011). Surrogate based optimization of a laidback fan-shaped hole for film-cooling. *International Journal of Heat and Fluid Flow*, 32(1), 226-238.
14. Schroeder, R.P. and Thole, K.A. (2016). Effect of high free stream turbulence on flow fields of shaped film cooling holes. *Journal of Turbomachinery*, 138(9), 1-10.
15. Rozati, A. and Tafti, D.K. (2008). Large-eddy simulations of leading edge film cooling: Analysis of flow structures, effectiveness, and heat transfer coefficient. *International Journal of Heat and Fluid Flow,* 29(1), 1-17.
16. KeYong, C.; Wei, C.; ShiQiang, L.; YongXian, G.; XiuLan, H. and XiaoHong, G. (2012). Film cooling with using the decomposition of an NH_3 cooling stream as a chemical heat sink. *Chinese Science Bulletin*, 57(27), 3652-3659.
17. Montomoli, F.; D'Ammaro, A. and Uchida, S. (2013). Numerical and experimental investigation of a new film cooling geometry with high P/D ratio. *International Journal of Heat and Mass Transfer*, 66, 366-375.
18. Johnson, B.; Tian, W.; Zhang, K. and Hu, H. (2014). An experimental study of density ratio effects on the film cooling injection from discrete holes by using PIV and PSP techniques. *International Journal of Heat and Mass Transfer,* 76, 337-349.
19. Nikpatro, A. and Schobeiri, M. T. (2016). Numerical and experimental investigation of aerodynamics on flow around a highly loaded low-pressure turbine blade with flow separation under steady and periodic unsteady inlet flow condition. *Proceedings of ASME Turbo Expo 2016: Turbomachinery Technical Conference and Exposition*, Paper No. GT2016-56699, V05AT13A010; 17 pages.
20. ANSYS User Manual Release 12 (2009), ANSYS Inc., USA